Metallomics

PAPER

View Article Online
View Journal | View Issue

Cite this: *Metallomics*, 2017, 9, 1622

Studies of copper trafficking in a mouse model of Alzheimer's disease by positron emission tomography: comparison of ^{64}Cu acetate and ^{64}CuGTSM†

Erica M. Andreozzi,‡[a] Julia Baguña Torres,‡[a] Kavitha Sunassee,[a] Joel Dunn,[a] Simon Walker-Samuel,[b] Istvan Szanda[a] and Philip J. Blower*[a]

Received 2nd August 2017,
Accepted 18th October 2017

DOI: 10.1039/c7mt00227k

rsc.li/metallomics

Alzheimer's disease can involve brain copper dyshomeostasis. We aimed to determine the effect of AD-like pathology on ^{64}Cu trafficking in mice, using positron emission tomography (PET imaging), during 24 hours after intravenous administration of ionic ^{64}Cu (Cu(II) acetate) and ^{64}Cu-GTSM ($GTSMH_2$ = glyoxalbis(thiosemicarbazone)). Copper trafficking was evaluated in 6–8-month-old and 13–15 month-old TASTPM transgenic and wild-type mice, by imaging 0–30 min and 24–25 h after intravenous administration of ^{64}Cu tracer. Regional ^{64}Cu distribution in brains was compared by *ex vivo* autoradiography to that of amyloid-β plaque. ^{64}Cu-acetate showed uptake in, and excretion through, liver and kidneys. There was minimal uptake in other tissues by 30 minutes, and little further change after 24 h. Radioactivity within brain was focussed in and around the ventricles and was significantly greater in younger mice. ^{64}CuGTSM was taken up in all tissues by 30 min, remaining high in brain but clearing substantially from other tissues by 24 h. Distribution in brain was not localised to specific regions. TASTPM mice showed no major changes in global or regional ^{64}Cu brain uptake compared to wildtype after administration of ^{64}Cu acetate (unlike ^{64}Cu-GTSM) but efflux of ^{64}Cu from brain by 24 h was slightly greater in 6–8 month-old TASTPM mice than in wildtype controls. Changes in copper trafficking associated with Alzheimer's-like pathology after administration of ionic ^{64}Cu are minor compared to those observed after administration of ^{64}Cu-GTSM. PET imaging with ^{64}Cu could help understand changes in brain copper dynamics in AD and underpin new clinical diagnostic imaging methods.

Significance to metallomics

The role of alterations in trafficking of copper, and other metals, as cause or consequence in dementias such as Alzheimer's is much discussed but poorly understood. This article focusses on acute changes in copper trafficking, particularly influx and efflux in brain, and how it is altered in a mouse model of Alzheimer's disease compared to normal mice, and highlights the growing opportunity to use positron emission tomography in the study of metallomics at the whole body level in animals and humans.

Introduction

Copper (Cu) is required by the body as a cofactor or regulator in many important physiological processes such as cell signaling, cellular respiration, free-radical defence, neurotransmitter synthesis, neuronal myelination, and iron metabolism.[1–4] Nevertheless, excess free Cu can be toxic because it catalyses reactions that generate free radicals, thus contributing to oxidative stress.[1,5] Consequently, various Cu transporters and Cu-binding proteins (*e.g.* Ctr1) play a crucial role in tightly regulating Cu trafficking at the cell and whole-body level. Incorrect function of these transporters and chaperone systems underlies inherited Cu metabolism disorders, such as Menkes disease and Wilson's disease, and may also occur in other pathological processes such as neurodegeneration and cancer.[5–10] In recent years, a growing body of evidence has associated Cu dysregulation with common neurodegenerative diseases, such as Alzheimer's disease (AD),[11–13] Parkinson's disease, Huntington's disease and amyotrophic lateral sclerosis (ALS). Although it is still unclear whether excess or deficiency of cellular Cu is a cause

[a] *Division of Imaging Sciences, Kings College London, St. Thomas Hospital, London, UK. E-mail: philip.blower@kcl.ac.uk*
[b] *UCL Centre for Advanced Biomedical Imaging, Division of Medicine, London, UK*

† Electronic supplementary information (ESI) available. See DOI: 10.1039/c7mt00227k

‡ These authors contributed equally.

or a consequence of these diseases, both *in vitro* and *in vivo* studies have confirmed the neurotoxic effects of Cu dysregulation.[5,14]

Several radioisotopes of Cu are available that could assist studies of trafficking and metabolism of Cu, although they have been used surprisingly infrequently for this purpose so far. The radiotracer approach is given added power by the growing availability of positron emission tomography (PET), which allows positron-emitting radioisotopes to be used to map acute copper trafficking processes across the whole body longitudinally and non-invasively in living humans and animals. Of the available positron-emitting copper radioisotopes, ^{64}Cu is the most practical due to its relatively long half life ($t_{1/2}$ = 12.7 h) which offers a relatively large time window (2–3 days) for PET imaging. As well as electron capture (43%) and beta-emission (39%) it decays by emission of a positron (18%) with low energy that is conducive to high-resolution PET imaging.[9] ^{64}Cu-PET has been used in rat models of Wilson's disease to show abnormalities in liver handling of copper after intravenous (IV) administration of a ^{64}Cu–histidine complex[15] or oral administration of ^{64}Cu chloride ($^{64}CuCl_2$).[10,16,17] There is also emerging interest in PET imaging of copper trafficking in cancer,[9,18,19] possibly related to changes in Ctr1 expression which affect resistance to chemotherapy.[1,20] Wang *et al.* investigated the influence of age on ^{67}Cu (administered as $^{67}CuCl_2$) uptake and distribution in mice using ^{67}Cu autoradiography and radioactivity measurements in cerebrospinal fluid (CSF) and explanted brain tissue, showing reduced active copper uptake, but increased total copper, in brains of older mice.[21] PET with ^{64}Cu in the form of the bis(thiosemicarbazone) complex Cu-GTSM (glyoxalbis(N^4-methyl-3-thiosemicarbazonato) copper(II)), a lipophilic bis(thiosemicarbazone) complex that delivers ^{64}Cu to all tissues and releases it within cells by a bioreductive mechanism, was used to show changes in copper retention. Tracking the distribution of radiocopper administered in different chemical forms and by different physiological routes is key to understanding the mechanisms of copper transport and distribution *in vivo* in health and disease and detecting potential alterations that might have diagnostic value.

In this paper, we compare trafficking of ^{64}Cu in a mouse model of AD-like amyloid-β plaque deposition with that in age-matched healthy control mice, during the first 24 h after administration of ionic ^{64}Cu (^{64}Cu-acetate) and ^{64}Cu-GTSM. Cu-GTSM (Fig. 1) is sufficiently lipophilic to penetrate the blood–brain barrier[22,23] and cell membranes, but has a relatively high Cu(II/I) redox potential which facilitates extremely rapid intracellular bioreduction and dissociation to release copper within cells,[24,25] irrespective of oxygenation status. In this respect, it differs from Cu-ATSM (Fig. 1), which requires a hypoxic environment for efficient bioreductive trapping.[24] Cu-GTSM was therefore expected to be non-specifically delivered to all well-perfused tissues including brain, bypassing physiological copper transporter systems and thus allowing monitoring of processes that involve efflux of copper from cells and tissues. Ionic Cu(II), on the other hand, was expected only to access cells by specific transport processes for "free" copper ions or those bound to plasma constituents. The resulting data may serve as a baseline for identifying changes in copper trafficking associated with disease states and evaluating whether PET imaging of such changes could form the basis of future clinical diagnostic methods.

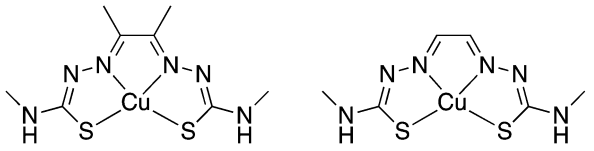

Fig. 1 Structures of bis(thiosemicarbazone) complexes Cu-ATSM and Cu-GTSM.

Methods

Radiochemistry

All reagents were purchased from Sigma-Aldrich, Alfa Aesar, Interlink Scientific Services or VWR International Ltd and used without further purification, unless otherwise stated. ^{64}Cu was produced as previously reported[26] in the form of copper-64 chloride ($^{64}CuCl_2$) in 0.1 N HCl solution (4.8 GBq μg^{-1}). ^{64}Cu-acetate was prepared by buffering $^{64}CuCl_2$ with a 3 M solution of sodium acetate to pH 6. ^{64}Cu-GTSM (radiochemical purity ≥95%, in physiological saline) was synthesised by reaction with H_2GTSM ligand as previously described (see ESI†).[23] Radiochemical purity was determined by thin layer chromatography using Merck 60 F_{254} silica gel plates and ethyl acetate as the mobile phase (R_f = 0.35, *cf.* R_f = 0 for $^{64}CuCl_2$ and ^{64}Cu-acetate).

PET imaging and biodistribution

All animal experiments were performed in accordance with the Animals (Scientific Procedures) Act, 1986 using protocols approved by the Animal Welfare and Ethical Review Body for King's College London (St Thomas' Campus). Animals were fed *ad libitum* with regular animal feed. Double-mutant male TASTPM mice on a C57BL/6J background were bred in-house from mice provided by GlaxoSmithKline (GSK), and genotyped to confirm the presence of the TAS and TPM mutant transgenes. TASTPM is a transgenic mouse model that rapidly develops some of the key pathologies associated with AD, including cerebral amyloid-β deposition, neuronal loss and neuroinflammation.[23] These mice exhibit impaired cognitive function by 6 months of age. Male C57BL/6J wildtype mice (6–8 months old), obtained from Charles River Laboratories International, Inc., were used as controls.

For blood clearance measurements, male TASTPM and age-matched control mice (n = 3 per group) were injected *via* a lateral tail vein with ^{64}Cu-GTSM or ^{64}Cu-acetate (8–10 MBq, ≤200 μL), and aliquots of blood (10 μL) were sampled from the left jugular vein at intervals from 1 to 60 min post-injection, weighed and gamma-counted. For PET imaging studies, animals were anaesthetised by isoflurane inhalation (3%, Vet Tech Solutions Ltd), and injected with ^{64}Cu-GTSM (n = 6) or ^{64}Cu-acetate (n = 4) in physiological saline *via* a lateral tail vein

(35–40 MBq, ≤200 μL). Respiration and temperature were monitored throughout all scans.

PET/CT imaging experiments were conducted using a nanoScan® PET/CT (Mediso Medical Imaging Systems, Budapest, Hungary), on mice in eight groups comprised as follows: Group 1: 6–8 month old TASTPM mice with ^{64}Cu-acetate (n = 3); Group 2: 6–8 month old control C57BL/6J mice with ^{64}Cu-acetate (n = 4); Group 3: 13–15 month old TASTPM mice with ^{64}Cu-acetate (n = 3); Group 4: 13–15 month old C57BL/6J mice with ^{64}Cu-acetate (n = 3); Group 5: 6–8 month old TASTPM mice with ^{64}Cu-GTSM (n = 6); Group 6: 6–8 month old control C57BL/6J mice with ^{64}Cu-GTSM (n = 4); Group 7: 13–15 month old TASTPM mice with ^{64}Cu-GTSM (n = 3); Group 8: 13–15 month old C57BL/6J mice with ^{64}Cu-GTSM (n = 3). Immediately after tail vein injection of the required tracer (35–40 MBq in ≤200 μL saline) the mice were placed on the scan bed in the prone position. Anaesthesia was maintained at 1.5–2% isoflurane throughout the scan. Whole-body PET imaging (400–600 keV energy window) was performed for the first 30 min post-administration, followed by a CT scan. Animals were then allowed to recover from anaesthesia and housed for 24 h with collection of urine and faeces. Mice were anaesthetised and re-scanned at 24 h post-injection for 1 h. On completion of scanning, (*i.e.* 25 h post-injection of tracer) mice were sacrificed by cervical dislocation and all major organs were explanted, weighed and gamma-counted (LKB Wallac 1282) to determine % ID per g. The total injected dose was defined as the sum of all whole-body counts (organs + carcass + excretion) excluding tail.

PET/CT datasets were reconstructed using three-dimensional iterative algorithms (8 iterations, 0.25 mm voxel size) and analysed using VivoQuant 1.21 software (InviCRO, LLC), co-registering PET and CT images and delineating regions of interest (ROIs) for quantification of activity in specific organs. For spine, heart, lung, liver and kidneys, a fixed volume of 20, 15, 15, 70 or 15 mm^3 respectively was drawn in a representative portion of the organ. The sum of activity (MBq) within each organ volume-of-interest (VOI) was divided by the sum of the whole body activity (determined from a VOI encompassing the whole body, excluding tail) and the VOI weight (assuming a density of 1 g mL^{-1}), yielding a representative value for organ % ID per mL. For measurements of global and regional brain uptake, a mouse brain atlas NM/CT module (InVICRO, LLC) was applied to all PET datasets. Brain ventricular uptake of ^{64}Cu was alternatively measured by drawing a spherical fixed-volume ROI (0.3125 mm^3) within the lateral ventricles. The mean and maximum concentration of activity per voxel in the ventricle ROI were divided by the ID normalised by the weight of the mouse to give mean and maximum standardised uptake values (SUV_{mean} and SUV_{max}), respectively. Colour scaling method for PET images is described in the ESI.†

Autoradiography and histology

Brains explanted from imaged mice killed 24 h after tracer injection, and a further group killed 48 h after injection, were immersed in 30% sucrose solution for 4 h and stored at −80 °C overnight, then sectioned (10 μm) sagittally using a Bright 5040 cryotome. The frozen sections were thaw-mounted onto Superfrost PLUS glass slides (Menzel-Glaser, Thermo Scientific), allowed to dry at room temperature and exposed to a storage phosphor screen (PerkinElmer, Super Resolution, 12.5 × 25.2 cm) in a standard X-ray cassette for 15 h. The phosphor screen was imaged using a Typhoon 8600 scanner (Molecular Dynamics) and the resulting images were analysed with OptiQuant 5.0 (PerkinElmer) and ImageJ (NIH).

Following autoradiography, the frozen slices were fixed (4% paraformaldehyde for 45 min), washed (distilled water), incubated in Congo red solution (0.5% Congo red dye [Sigma Aldrich] in 50% EtOH) for 15–20 min (to visualise amyloid plaques), rinsed (distilled water), dipped 5–10 times in alkaline alcohol (1% NaOH, 50% EtOH), rinsed (water, 1 min), counter-stained with Harris' haematoxylin [Sigma Aldrich] for 10 s, rinsed (water) for 2 min, dehydrated (1 mL 3 M HCl in 200 mL 70% IMS for 1 min; 95% alcohol for 3 min, 2 changes; 100% alcohol for 3 min, 2 changes), cleared (Histo-Clear II solution [National Diagnostics] twice for 1 min each), and mounted with DPX new mounting medium (Merck Millipore). Sections were evaluated under bright-field using a DM6000 B microscope (Leica Microsystems Ltd, Bucks, UK). Autoradiographic and histological images were co-registered with software created in-house (PhosphorCount[27]) using the Interactive Data Language (IDL, Boulder, CO). The histology image (bright field photomicrograph) and corresponding phosphorimage (autoradiograph) were sequentially loaded onto the Phosphorcount program as GEL and TIFF files respectively. The histological images were resampled to match the lower resolution of the autoradiographs, and the paired images were co-registered by maximising the mutual information measure for the two images, generating an 'overlay' image in which each pixel of the autoradiograph was associated with a corresponding pixel from the histology image. Regions of interest (ROI) were then drawn to measure the autoradiographic signal (phosphor counts per mm^2) residing in the lateral ventricle, other brain regions, and the whole brain.

Statistical analysis

Statistical analysis was performed using GraphPad Prism 5 (GraphPad Software Inc.) and SPSS (IBM Corp.). In GraphPad, data were analysed with two-way ANOVA and Bonferroni multiple comparison *post hoc* tests and with one-way ANOVA with Dunnett's multiple comparison *post hoc* tests. In SPSS, data were analysed with a three-way ANOVA and multiple comparison *post hoc* tests. P values <0.05 were considered statistically significant.

Results

Comparison of ^{64}Cu-acetate and ^{64}Cu-GTSM

The clearance of radioactivity from blood was investigated using blood sampled from the jugular vein following intravenous injection of ^{64}Cu-GTSM or ^{64}Cu-acetate. Both tracers showed rapid bi-exponential clearance (Fig. 2); ^{64}Cu-GTSM has a very rapid initial clearance phase with half-life ≪1 min (at least 80%

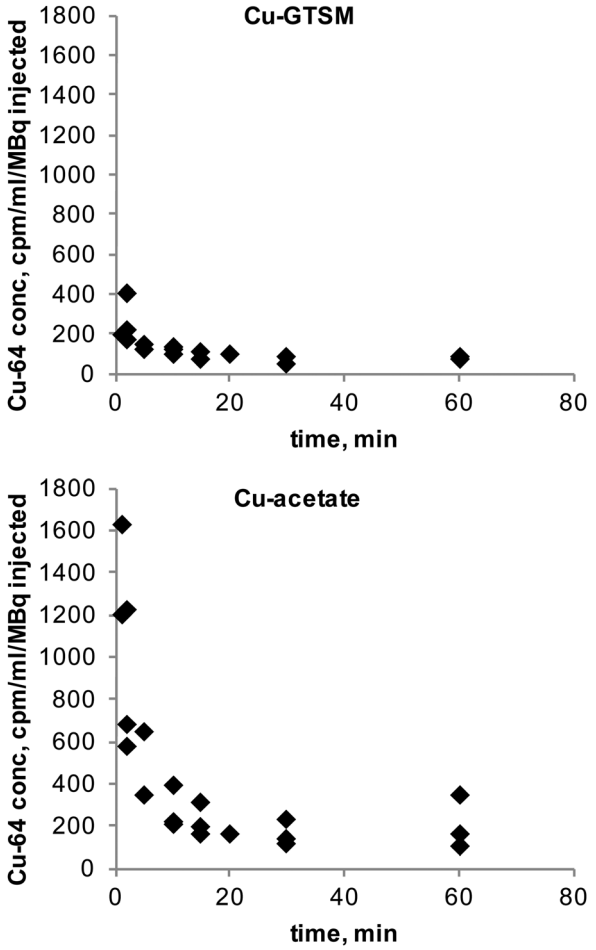

Fig. 2 Blood radioactivity concentration (relative to injected dose, cpm/μL/MBq injected) curves of ^{64}Cu in 6–8-month-old C57BL6J mice following IV administration of ^{64}Cu-GTSM (n = 3, top) and ^{64}Cu-acetate (n = 3, bottom). Initial clearance of Cu-GTSM is very rapid with half-life <1 min, whereas Cu-acetate has a slower initial clearance with half-life *ca.* 2–3 min. Both tracers show a prolonged slow clearance phase following initial rapid clearance.

of radioactivity had cleared before the first samples were taken at 1–2 min post injection), while ^{64}Cu-acetate has an early phase half-life of 2–3 min. Both tracers show a second very slow clearance phase, with ^{64}Cu-GTSM reaching lower blood levels than ^{64}Cu(II) acetate by 1 h.

PET imaging in 6–8 month-old wild-type mice at both 30 min and 24 h showed marked differences in whole body distribution of ^{64}Cu after intravenous administration, between ^{64}Cu-acetate and ^{64}Cu-GTSM in normal mice (Fig. 3). At 30 min, mice injected with ^{64}Cu-acetate (Fig. 3a) showed ^{64}Cu accumulation in the liver, kidneys, and intestines. ^{64}Cu-GTSM (Fig. 3b), on the other hand, while also showing ^{64}Cu accumulation in the liver, kidneys and intestines, exhibited high uptake in lungs, heart, brain and spinal cord. The adrenal glands were also prominent on the images. After 24 h, the activity in the lungs, kidneys, heart and adrenals, but not brain, had decreased considerably compared to liver and intestines (Fig. 3b, Fig. 4). For ^{64}Cu-acetate, by contrast, there was relatively little change in gross organ biodistribution between 30 min and 24 h (Fig. 3a, Fig. 4). Images obtained with the respective tracers in 13–15 month-old wild-type mice, and in TASTPM mice in both age groups, showed similar trends.

These qualitative impressions were supported by quantitative analysis of the whole body PET images. The % ID per mL of ^{64}Cu in heart, lungs, kidneys, brain and spinal cord was significantly higher ($p < 0.001$) for ^{64}Cu-GTSM than for ^{64}Cu-acetate at both 30 min and 24 h (Fig. 4a and Fig. S3, S4 and Table S1, ESI†). This indicates more efficient extraction into tissues from blood in the case of ^{64}Cu-GTSM, consistent with its faster initial clearance from blood (*vide supra*). While %ID per mL for ^{64}Cu-GTSM in liver at 30 min was slightly lower than for ^{64}Cu-acetate, it increased with time (while decreasing in the case of ^{64}Cu-acetate) and by 24 h was similar for the two tracers. It is particularly notable that % ID per mL in heart, lung and brain at 30 min were higher for ^{64}Cu-GTSM than ^{64}Cu-acetate by factors of 8.4, 6.2 and 8.2 respectively. While % ID per mL values for ^{64}Cu-GTSM in heart and lungs fell by 57% and 71% respectively between 30 min and 24 h they still remained higher at 24 h than those for ^{64}Cu-acetate, by factors of 5.3 and 2.2, respectively. By contrast with these organs, the high uptake of ^{64}Cu-GTSM in brain at 30 min (5.57 ± 0.77% ID per mL) did not fall significantly by 24 h (5.45 ± 0.75% ID per mL). These differences between ^{64}Cu-acetate and ^{64}Cu-GTSM were confirmed by *ex vivo* biodistribution measurements on explanted organs at 24 h (Fig. 4b).

To examine the distribution of the tracers in brains of mice in more detail, PET (Fig. 5) and digital autoradiography (*vide infra*, Fig. 6) were employed. Quantitative PET imaging of normal mice showed that ^{64}Cu-GTSM delivered ^{64}Cu to all parts of the brain very efficiently by 30 min (5.57 ± 0.77% ID per mL, n = 6), with almost complete retention at 24 h (5.45 ± 0.75% ID per mL, n = 6) and only minor variations in concentration in different regions (Fig. 5). Mapping the images onto a 3D anatomical digital brain atlas confirmed small but significant differences between regions. By contrast, ^{64}Cu-acetate delivered a much smaller fraction of activity to brain from blood by 30 min (0.73 ± 0.03% ID per mL) and did so in a highly focal manner, with radioactivity localised selectively in the regions around the ventricles (Fig. 5), and to a lesser extent in the hypothalamus (detected by autoradiography, see Fig. 6), while in other regions uptake was much lower (averaging <0.75% ID per mL). Although regional PET quantification by co-registration with the brain atlas yielded ~1.5% ID per mL for periventriclular uptake of ^{64}Cu-acetate (Table S1 and Fig. S5, ESI†), the PET images show that this is grossly underestimated both because the regions in question are not adequately resolved and hence subject to partial volume effects, and because of poor registration (for example, the atlas does not include the fourth ventricle (FV)). Therefore we also compared the uptake in the ventricular regions with that in a "background" brain region (frontal cortex) using the SUV_{max} parameter, which although potentially more affected by noise, is less dependent on correct mapping of regions of interest and somewhat less affected by partial volume effects. By this parameter, periventricular uptake (SUV_{max} in range 0.5–1.5 at 30 min, *i.e.* close to the average for the whole body)

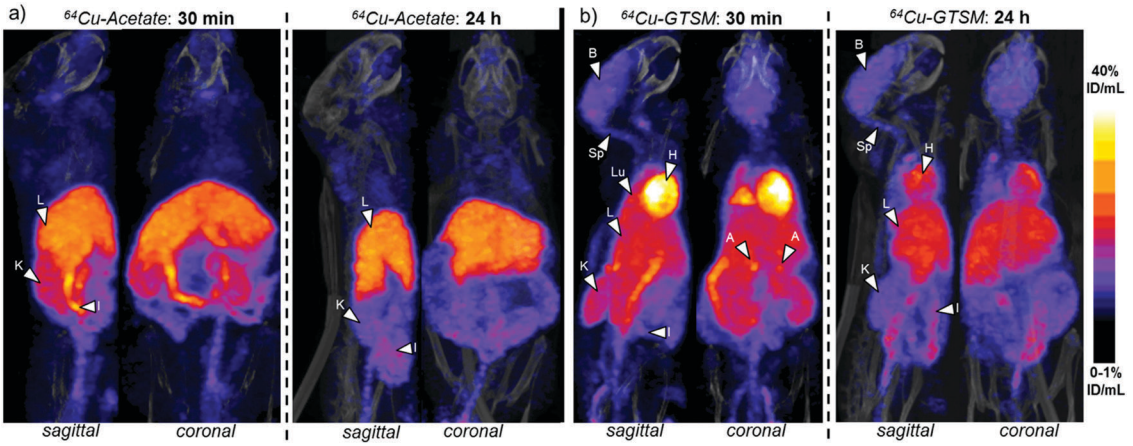

Fig. 3 Sagittal and coronal views of PET/CT maximum intensity projections (MIPs) of 6–8-month-old C57BL/6J wild-type mice at 30 min and 24 h post-injection of ^{64}Cu-acetate (a) and ^{64}Cu-GTSM (b). ^{64}Cu-acetate PET/CT scans revealed extensive tracer accumulation in the liver, intestines and kidneys and very low uptake in the brain at both imaging time points; ^{64}Cu-GTSM showed high uptake in the liver, intestines, kidneys and was also taken up avidly by the brain, heart, lungs and adrenal glands. A significant fraction of the radioactivity in heart, lungs, kidney and adrenals, but not brain, had cleared by 24 h. Arrows: A = adrenal glands; H = heart; L = liver; K = kidneys; I = intestines; B = brain; Sp = spine; Lu = lungs. The colour scale is linear, covering the range 0–1% ID per mL (min) to 40% ID per mL (max).

was at least an order of magnitude higher than in the reference region (<0.1).

For both ^{64}Cu-GTSM and ^{64}Cu-acetate, clearance of ^{64}Cu from total brain and spinal cord between 30 min and 24 h was less ($>98\%$ retained) than from other tissues (Fig. 4) and there was no obvious redistribution between different brain regions between 30 min and 24 h. Measurement of clearance of ^{64}Cu-acetate from the periventricular regions between 30 min and 24 h was unreliable because of their irregular shape and small size, and the resulting difficulty in co-registering the 30 min and 24 h images with sufficient accuracy; dramatic clearance or redistribution was not observed.

Digital autoradiography of brain sections at 24 h (Fig. 6) confirmed the strongly contrasting regional distribution of ^{64}Cu delivered as ^{64}Cu-GTSM and ^{64}Cu-acetate, and showed that qualitatively the focal distribution around the ventricles and hypothalamus associated with ^{64}Cu-acetate was at least partially maintained 48 post injection. Digital autoradiography offers higher resolution than nanoPET, and by careful co-registration both manually and objectively using a computer algorithm[27] of autoradiographs stained micrographs of the same section, it was possible to show that the increased activity evident on the PET scans in the ventricular regions arises from increased ^{64}Cu concentration both within the ventricular space or choroid plexus and in the immediate sub-ventricular tissue (fimbria, see Fig. 6).

Comparison of AD and wild-type mice

To assess possible changes in brain trafficking of ionic copper associated with AD, and compare them with previously observed[23] significant changes in ^{64}Cu-GTSM distribution, the fate of intravenously administered ^{64}Cu-acetate was monitored longitudinally by PET in 6–8 and 13–15 month-old male TASTPM mice and age-matched controls. The general biodistribution of the tracer among organs and tissues other than brain was similar in 6–8 month- and 13–15 month-old TASTPM mice. Details of the quantitative comparison based on PET image analysis and *ex vivo* biodistribution, including some minor but potentially significant differences in uptake and clearance of heart, spine, liver and kidneys that warrant further investigation, are shown in Fig. 7. Quantitative PET image analysis and *ex vivo* counting revealed no significant differences in global brain ^{64}Cu concentration (% ID per g) between TASTPM transgenic mice and wild-type controls injected with ^{64}Cu-acetate in either age group. However, both PET and gamma-counting demonstrated an age-dependent decrease in global brain ^{64}Cu concentration between 6–8 months and 13–15 months, in both TASTPM transgenic mice and controls. These findings are consistent with those of Wang and co-workers, who reported an age-related reduction of brain $^{67}CuCl_2$ uptake in C57BL/6J wildtype mice.[21]

Tracking the efflux of ^{64}Cu administered as ^{64}Cu-acetate from the brain of each individual mouse in each group between 30 min and 24 h revealed that in 6–8 month TASTPM mice, efflux of radioactivity from brain was significant: $9.13\% \pm 1.28\%$ ($n = 3$) of the total brain activity at 30 min was lost by 24 h in the AD mice (group 1; see Fig. 7 and Fig. S7, ESI†). In their age-matched wild-type counterparts, on the other hand (group 2), there was no significant efflux (total brain radioactivity increased by $2.4\% \pm 5.6\%$, $n = 4$). Efflux from the spinal cord was also greater in TASTPM mice than controls (28.5 ± 2.7 *vs.* $16.5 \pm 4.8\%$ decrease in spine % ID per mL). This difference in efflux was not found in the brains of 13–15 month old mice where ^{64}Cu concentration in brain did not change significantly over time for both TASTPM and control mice ($2.3\% \pm 4.3$ and $1.5\% \pm 5.6\%$ in % ID per mL), respectively.

The distribution of radioactivity within the brains of TASTPM mice was measured both by PET imaging and digital autoradiography. It was found to be similar both to that reported above for wild-type mice and to that in the age-matched wild type groups

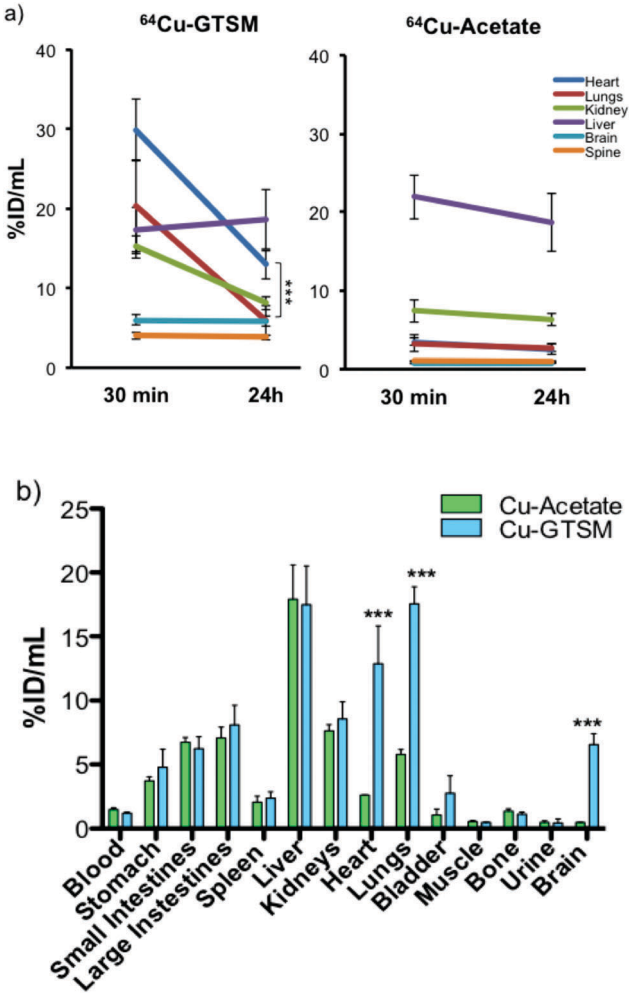

Fig. 4 (a) Time-dependent ROI analysis of whole body PET of 6–8 month-old wild-type mice showing ^{64}Cu uptake (% ID per mL) in, and clearance from, major organs (heart, lungs, kidney, liver, brain, and spine) after ^{64}Cu-GTSM and ^{64}Cu-acetate administration. The uptake of ^{64}Cu in all organs except liver (and blood, see Fig. 2) was significantly higher ($p < 0.001$) for ^{64}Cu-GTSM than for ^{64}Cu-acetate at both 30 min and 24 h. In the case of ^{64}Cu-GTSM, there is dramatic clearance of activity between 30 min and 24 h from heart, lungs, and kidney but not brain and spinal cord. Clearance of activity from brain and spinal cord was also absent or notably slower than from other tissues in the case of ^{64}Cu-acetate. Data shown are mean ± SD (n = 4 for ^{64}Cu-acetate; n = 6 for ^{64}Cu-GTSM). (b) *Ex vivo* tissue biodistribution of ^{64}Cu in 6–8-month-old C57BL6J mice at 24 h post-injection of ^{64}Cu-GTSM and ^{64}Cu-acetate. Statistically significant differences between the two tracers are indicated by *** ($p < 0.001$). Data are mean ± SD (n = 3 for ^{64}Cu-acetate; n = 6 for ^{64}Cu-GTSM).

at both 6–8 months and 13–15 months of age, that is, radioactivity was mainly located around the ventricles (Fig. 8) in both age groups, and there were no significant differences in regional distribution by age or disease. However, because of the small size and irregular shape of these regions, only very major difference between age groups and between TASTPM and controls would have been detected. The spatial distribution of ^{64}Cu in the autoradiographs showed no obvious correlation with the spatial distribution of amyloid plaques seen by Congo red staining of nearby sections (Fig. 8).

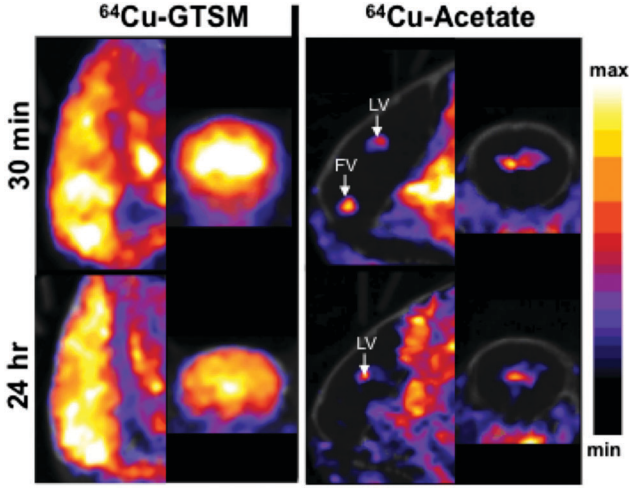

Fig. 5 Representative (of n = 4 for ^{64}Cu-acetate; n = 6 for ^{64}Cu-GTSM) coronal and sagittal (anterior towards the top of the images) slices though PET/CT reconstructions illustrating ^{64}Cu distribution in the brains of a 6–8-month-old C57BL/6J mice at 30 min (top) and 24 h (bottom) post-injection of ^{64}Cu-GTSM (left) and ^{64}Cu-acetate (right). White arrows identify lateral ventricles (LV) and fourth ventricle (FV).

Discussion

Cu-GTSM and Cu-acetate show strikingly different *in vivo* behaviour and biodistribution. Cu-GTSM has a significantly shorter early-phase half-life of extraction from blood than Cu-acetate, and efficient uptake in all major organs, including brain and most prominently liver, kidneys, heart, lungs and adrenals, by 30 minutes post-injection. The short early-phase blood clearance of both tracers, combined with the absence of prominent blood pool signal on the PET images at 30 minutes, indicates that the prominent signal in several organs reflects uptake into the cells of these tissues and not their blood content. By contrast with ^{64}CuGTSM, ^{64}Cu-acetate is only efficiently taken up in kidneys and liver (with subsequent rapid transfer to the gut, consistent with earlier reports of rodent experiments[28–30]) and not in other organs. Another copper bisthiosemicarbazone complex, ^{61}Cu-PTSM, has also shown higher uptake into brain (and other tissues) than ionic copper in rats (although less prominently than ^{64}Cu-GTSM, and with washout within 2 h).[31]

This direct comparison and distinct behaviour of ^{64}Cu-GTSM and ionic ^{64}Cu is important for several reasons. Recent reports have highlighted the similarity of biodistribution of copper bisthiosemicarbazone complexes such as ^{64}Cu-ATSM with that of ionic ^{64}Cu, leading to suggestions that the bisthiosemicarbazone complexes release ionic copper rapidly and that the biodistribution consequently observed is essentially that of ionic copper.[29] The present results suggest that this is not the case and support the hypothesis that ^{64}Cu-GTSM delivers its copper payload directly across cell membranes and the blood brain barrier, bypassing native specific or active transport mechanisms and bioreductively releasing ^{64}Cu inside cells. The failure of ^{64}Cu-ATSM to deliver ^{64}Cu efficiently to brain and heart (shared by ionic ^{64}Cu)[22,29] can be explained by the hypoxia-selectivity of the Cu-ATSM complex

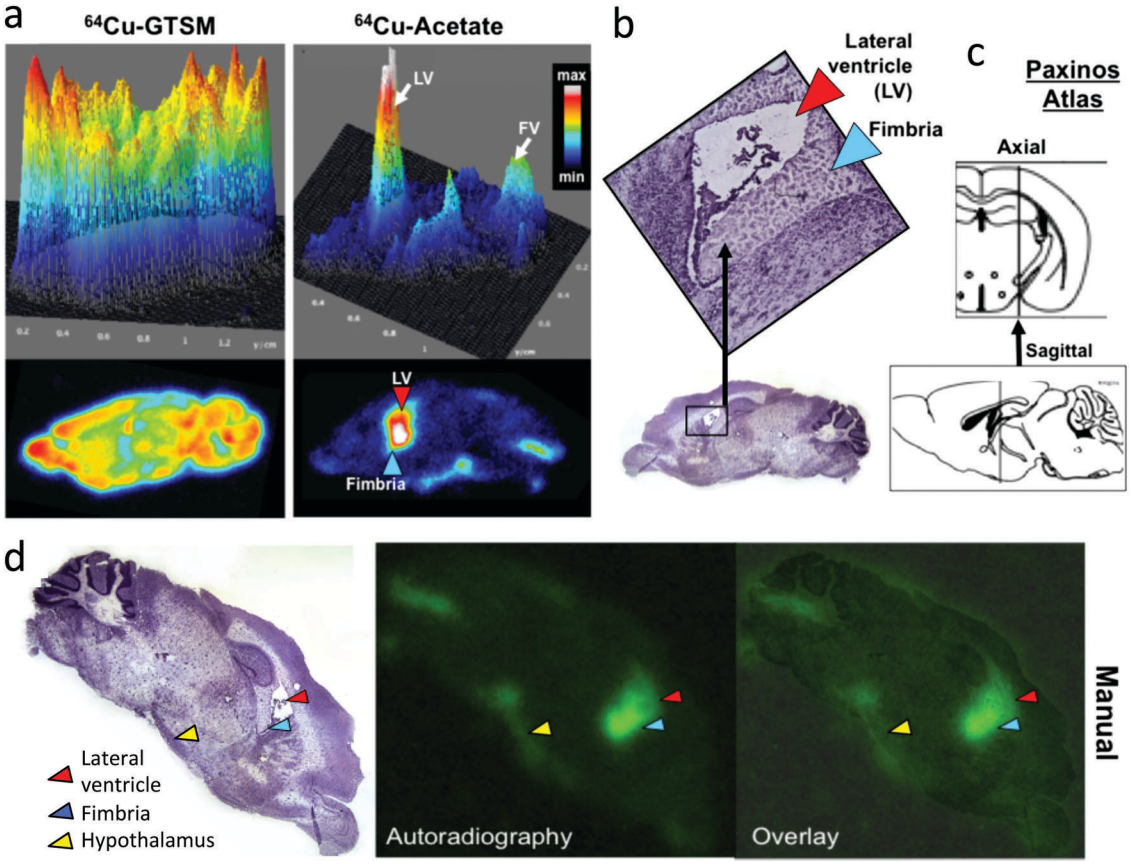

Fig. 6 (a) Representative digital autoradiographs and corresponding surface plots of a brain tissue slice at 24 h post injection of ^{64}Cu-GTSM and ^{64}Cu-acetate in a 6–8 month-old wild-type C57BL/6J mouse. ^{64}Cu-GTSM (left) demonstrates higher and more uniform signal distribution than ^{64}Cu-acetate (right), which shows distinct focal accumulations in and around the lateral and fourth ventricles (white arrows in surface plot) and to a lesser extent the hypothalamus. The location of the lateral ventricle (LV) and fimbria are indicated in the digital autoradiograph with arrows. (b) Photomicrograph of the stained (haematoxylin) tissue section corresponding to (a), providing anatomical reference for identifying key regions (lateral ventricles, red arrow, hippocampal fimbria, blue arrow) exhibiting high uptake. (c) Anatomical diagram from the Paxinos brain atlas indicating the approximate location of the sagittal section in (a) and (b), lying between the third and lateral ventricle, about 1.44 mm lateral to bregma. (d) manual co-registration (overlay) of histology and autoradiography images corresponding to the same tissue slice (left: haematoxylin stained tissue section micrograph showing the lateral ventricle (red arrow), hippocampal fimbria (blue arrow) and hypothalamus (yellow arrow); centre: autoradiograph; right: overlay).

due to its low reduction potential and slow dissociation post-reduction. Cu-GTSM is more readily reduced and dissociates more quickly after reduction and is consequently not hypoxia-selective and releases copper much more efficiently within cells. The rapid release of ^{64}Cu within brain by this mechanism[32] was supported by the observation that by 30 minutes, none of the brain copper remained in the form of Cu-GTSM.[23] The present results show that, by contrast, ionic ^{64}Cu is unable to enter most parts of the brain to a significant degree (and likewise other tissues with a high avidity for Cu-GTSM, including heart, lungs and adrenals). The contrast in biodistribution between ^{64}Cu-acetate and ^{64}Cu-GTSM vindicates both the choice of Cu-GTSM to begin studies of copper trafficking in disease and the hypothesis that studies of the biodistribution of ionic ^{64}Cu alone are insufficient to understand such processes. Intravenous injection of ^{64}Cu-acetate will lead to binding with some blood-borne copper carrier proteins, and the rate at which these equilibria are reached, compared to the rate of transport of blood to the target tissues, is not well established.[1,33–35] Previous studies show that the blood half-life was changed very little when ^{67}Cu-acetate was incubated with human serum albumin (HS) before injection;[28] and it has been shown that there is much higher uptake in rat brain tissue at 4 h when ^{67}Cu is administered intravenously in the form of ^{67}Cu(II)–nitrilotriacetate, ^{64}Cu-chloride or ^{64}Cu-albumin compared to $^{64/67}$Cu(II)–ceruloplasmin sources,[35,36] suggesting that ceruloplasmin has at most a minor role in Cu transport to brain tissue. Thus, studies with several different chemical forms (including plasma protein carriers such as albumin, transcuprein and ceruloplasmin[35]) and routes of administration will be required to identify which are directly involved in delivery to specific tissues.

The distribution of the two tracers within brain is strikingly different: ^{64}Cu-GTSM has a high level of uptake throughout the brain while Cu-acetate has very low overall brain uptake which is confined to focal regions around the ventricles and hypothalamus.

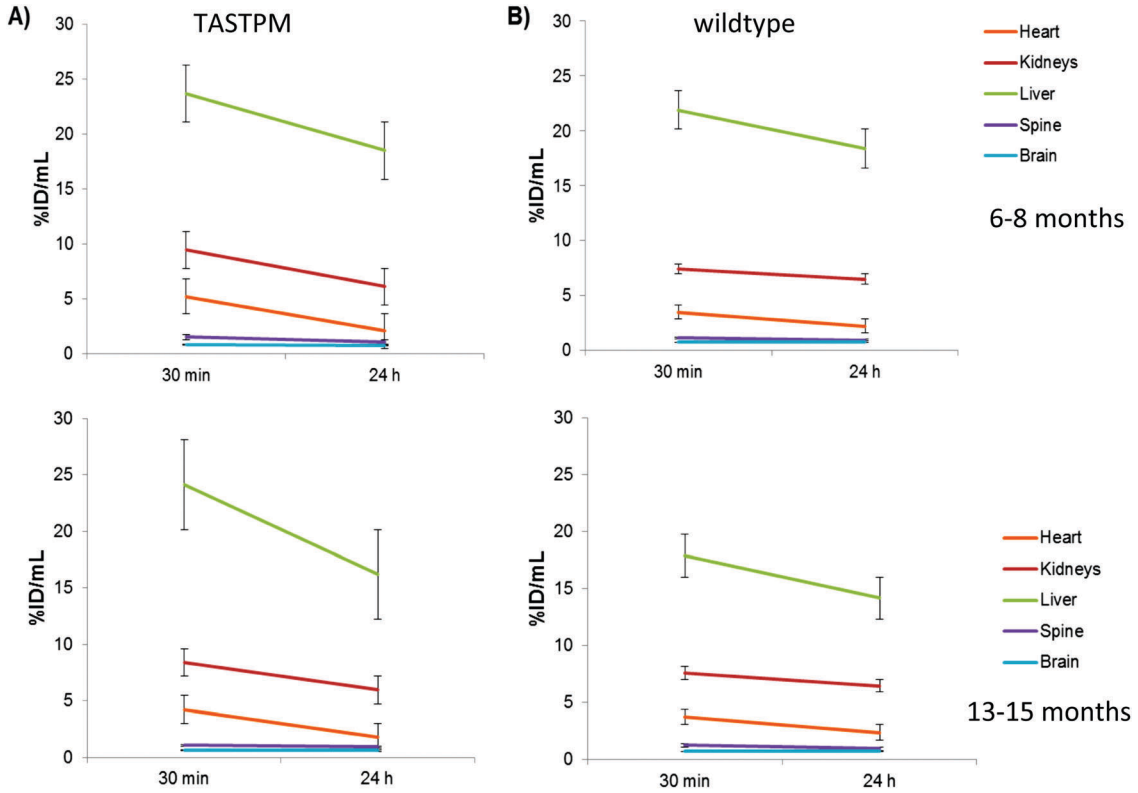

Fig. 7 Time-activity curves extracted from PET image analysis showing changes in ^{64}Cu concentration (expressed as % ID per mL, after intravenous administration of ^{64}Cu-acetate) between 30 min and 24 h in the whole heart, kidneys, liver, spine and brain of 6–8-month-old (top) and 13–15 month-old (bottom) male TASTPM mice (left) and age-matched C57BL/6J controls (right). Data are mean (n = 3 for all groups except n = 4 for 6–8 month-old wildtype controls) ± SEM.

The focal uptake of ^{64}Cu around the ventricles following ^{64}Cu-acetate injection is consistent with some previous observations showing preferential uptake of radioactive copper in choroid plexus compared to other brain regions shortly after intravenous administration in various chemical forms.[36] Studies in our laboratory by X-ray fluorescence[37] have shown that the total concentration of endogenous copper is significantly higher in periventricular tissues (such as choroid plexus) than in other brain regions. Similarly, others have shown by XRF that local Cu concentrations were thousands of times higher in astrocytes of the subventricular zone compared to other cells,[38] and by laser ablation-inductively coupled plasma-mass spectrometry (LA-ICPMS)[39] that copper levels in the choroid plexus where higher than in other regions. The observation that the localisation of acute uptake in the periventricular region (by radionuclide tracking) spatially matches the chronic accumulated copper concentration (by XRF and LA-ICPMS) may be significant and suggests the possibility of rapid equilibration between incoming copper and the stored copper pool, which deserves further investigation. It is notable that these regions match the preferential expression of several genes implicated in copper transport and storage: high ceruloplasmin gene expression in astrocytes was suggested as a likely explanation for high Cu content in the choroid plexus in C57BL6/7 mice,[39] while mRNA encoding Cu transporter-1 (Ctr1) and ATP7A was higher in the choroid plexus than in brain capillaries and parenchyma. Similarly, metallothionein was localised preferentially in the choroid plexus epithelium compared to other parts of the rat and mouse brain.[3,40] On the other hand, ATP7B mRNA was particularly high in the hypothalamus.[41] The resolution of the present studies, both spatially and temporally, coupled with the small size and irregular shape of the ventricles in mice, limits more detailed interpretation of the available data. However, dynamic PET with ^{64}Cu in humans would allow more precise spatial and temporal mapping of copper trafficking in these small brain regions, unhampered by the effects of general anaesthesia, and would help to determine whether the behaviour we and others have observed reflects a possible role of cerebrospinal fluid, choroid plexus and surrounding tissues as a gateway and regulator for copper storage and transport into and out of the brain.

Another striking observation is that while acutely delivered ^{64}Cu administered as ^{64}CuGTSM is partially cleared from most tissues (Fig. 4a) in normal mice between 30 min and 24 h, ^{64}Cu administered as ^{64}Cu-acetate clearance from these tissues is much less. Notably, there is no significant clearance of radioactivity from brain of either tracer. This represents a difference between brain and other tissues that is even more marked than that seen in an earlier PET study in humans using another copper bisthiosemicarbazone complex, ^{62}Cu-PTSM, where the biological half-life of radioactivity in brain was longer than in heart and other organs.[42–44] The significance of this unique

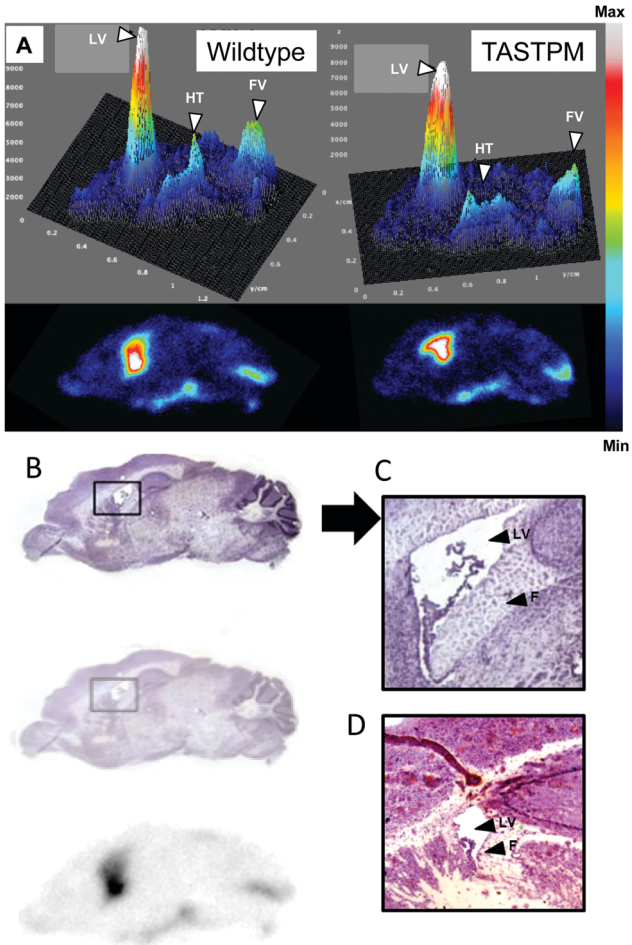

Fig. 8 (A) *Ex vivo* brain autoradiographs and corresponding surface plots from representative sagittal brain sections of 6–8 month-old wild-type (left) and TASTPM (right) mice sacrificed at 24 h post-injection of ^{64}Cu-acetate. *Ex vivo* autoradiography revealed a similar pattern of ^{64}Cu accumulation in the brain for both control and AD mice, with main radioactive hotspots situated around the lateral and fourth ventricles and hypothalamus. LV = lateral ventricle; FV = fourth ventricle; HT = hypothalamus. (B) Photomicrograph of sagittal brain section, stained with haematoxylin, from a 6–8-month old wildtype mouse (top), corresponding autoradiograph (bottom) and overlay (centre) at 24 h post-injection of ^{64}Cu-acetate; (C) magnified view of the area surrounding the lateral ventricle in haematoxylin-stained brain section shown at B; (D) magnified view of the lateral ventricle area in a nearby sagittal brain slice, stained with Congo red dye to visualise amyloid plaques, from a 6–8 month old TASTPM mouse. None of the regions showing high ^{64}Cu signal on the autoradiographs exhibited significant Aβ plaque deposition. LV = lateral ventricle; F = fimbria of the hippocampus.

behaviour of brain is unclear at present; it could be interpreted as suggesting that the healthy brain lacks a functional mechanism to export copper, a hypothesis that deserves further investigation in the context of copper trafficking in health and dementia.

Comparison of the TASTPM Alzheimer's disease model mice with their normal age-matched counterparts as a group showed no obvious difference in mean global brain uptake of ^{64}Cu-acetate, or its spatial distribution within the brain, in contrast to the marked differences observed previously with ^{64}Cu-GTSM. The design of this experiment also allowed comparison of young (6–8 months) mice with older (13–15 months) mice. This showed that both in the wild-type and TASTPM groups, global brain uptake of ^{64}Cu-acetate was significantly higher in the younger mice, consistent with a previous report using ^{67}Cu-chloride.[21] The reduction with age in acute uptake contrasts with the results of measurements of total brain copper by XRF,[21] which showed significantly more copper in the brains of older mice. This could be interpreted in numerous ways, but may indicate a level of regulation of uptake related to the availability of and demand for copper within the brain.

Using ^{64}CuGTSM for ^{64}Cu delivery, efflux between 30 minutes and 24 h was significantly increased in TASTPM mice compared to wild type.[23] A similar comparison here with ^{64}Cu-acetate was more equivocal. There was no significant difference in average brain uptake between TASTPM and wildtype groups at either 30 min and 24 h; however, when the % clearance from brain between 30 min and 24 h was calculated for individual mice (taking advantage of the statistical advantage due to the inherent pairing of data), a trend towards greater clearance in the TASTPM mice was evident, although only in the 6–8 month age group: the % change of brain activity between 30 min and 24 h ranged from −10.0% to −8.2% in the TASTPM mice and from −2.4% to +9.0% in the wildtype mice. In the older age group, on the other hand, the respective ranges were −1.7% to +10.6% and −6.8% to +6.7% (shown graphically in ESI,† Fig. S7). The clearance of ^{64}Cu from brain after the initial uptake deserves further investigation, including in humans, both to understand difference in copper efflux mechanisms between brain and other tissues, and to determine their relationship with age and Alzheimer's pathology.

The TASTPM mice exhibited the formation of amyloid plaques, detectable by Congo red staining, in several brain regions, but as previously observed for ^{64}Cu-GTSM,[23] those regions were not among those showing the highest uptake of ^{64}Cu-acetate; in particular, the periventricular regions did not show particularly abundant plaque formation. In other parts of the brain, while ^{64}Cu-GTSM showed a lack of spatial correlation (or even a negative correlation) between ^{64}Cu uptake and plaque abundance,[23] subtle variation in ^{64}Cu uptake after ^{64}Cu-acetate administration could not easily be measured or correlated with amyloid abundance because of low uptake. The lack of spatial correlation of ^{64}Cu uptake with plaque abundance seen for either ^{64}Cu-acetate or ^{64}Cu-GTSM does not support the hypothesis that amyloid plaques sequester significant amounts of copper. This could be explained on the basis that mouse amyloid plaques do not sequester copper, or that the amyloid-bound copper is not rapidly exchangeable with exogenous copper.

Conclusion

^{64}Cu-GTSM and ^{64}Cu-acetate show contrasting biodistributions and blood clearance rates, and ^{64}Cu bisthiosemicarbazone complexes do not simply reflect the biodistribution of ionic copper. Whereas ^{64}Cu-GTSM crosses the blood brain barrier

and delivers substantial ^{64}Cu activity to all parts of the brain, ^{64}Cu-acetate delivers significant amounts of ^{64}Cu only to the periventricular regions and the hypothalamus, suggesting that further investigation of the routes by which the brain acquires its essential copper could usefully focus on these regions. Global brain uptake of ^{64}Cu-acetate was significantly higher in the younger mice than in the older ones. Clearance of ^{64}Cu from brains of normal mice up to 24 h after delivery in the form of ^{64}Cu-acetate was insignificant, in contrast to clearance from other tissues. In this respect ^{64}Cu-acetate resembles ^{64}Cu-GTSM, suggesting that the normal brain lacks a functional mechanism to allow efflux of copper. In young (6–8 weeks) TASTPM mice given ^{64}Cu-acetate, by contrast, there is a trend towards greater efflux from brain, but further experiments would be required to confirm the significance of this trend and hence determine whether, in this respect too, ^{64}Cu-acetate resembles ^{64}Cu-GTSM and hence whether the genetic modifications in TASTPM mice that underlie their mimicry of AD pathology also modify the brain's ability, or need, to export copper. There was no spatial correlation of ^{64}Cu uptake with amyloid plaque abundance after administration of ^{64}Cu-acetate. Using PET to study the biodistribution of ^{64}Cu offers a powerful tool to study the role of copper trafficking abnormalities in diseases including dementia, potentially leading to valuable new diagnostics, but administration of only ionic ^{64}Cu intravenously is insufficient to understand such processes and other chemical forms and administration routes must be studied.

Conflicts of interest

There are no conflicts to declare.

Acknowledgements

This research was supported by the Alzheimer's Society (studentship to JBT), Alzheimer's Research UK (ARUK), and King's Health Partners (KHP) Research Challenge Fund, the Centre of Excellence in Medical Engineering funded by the Wellcome Trust and EPSRC under grant number WT088641/Z/09/Z, the King's College London and UCL Comprehensive Cancer Imaging Centre funded by CRUK and EPSRC in association with the MRC and DoH (England), and by the National Institute for Health Research (NIH) Biomedical Research Centre at Guy's and St Thomas' NHS Foundation Trust and King's College London. EMA was supported by a Whitaker International Program Fellowship. PET and SPECT scanning equipment was funded by an equipment grant from the Wellcome Trust. We thank Dr Karen Shaw and Dr Zilin Yu for the production of $^{64}CuCl_2$, Mr Stephen Clark for assistance and advice in animal experiments and PET scanning, and Dr Ciara Finucane for assistance with InVicro's brain atlas software. We thank Dr Vineeth Rajikumar and Dr Kazumi Chia for their assistance with the Phosphorcount program for co-registration of autoradiography and histology. We thank GSK for providing animals from which the TASTPM mouse colony was derived. The views expressed are those of the authors and not necessarily those of the NHS, the NIHR or the Department of Health.

References

1 S. Lutsenko, A. Bhattacharjee and A. L. Hubbard, Copper handling machinery of the brain, *Metallomics*, 2010, **2**, 596–608.
2 K. M. Davies, D. J. Hare, V. Cottam, N. Chen, L. Hilgers, G. Halliday, J. F. B. Mercer and K. L. Double, Localization of copper and copper transporters in the human brain, *Metallomics*, 2013, **5**, 43–51.
3 I. F. Scheiber, J. F. B. Mercer and R. Dringen, Metabolism and functions of copper in brain, *Prog. Neurobiol.*, 2014, **116**, 33–57.
4 V. Desai and S. G. Kaler, Role of copper in human neurological disorders, *Am. J. Clin. Nutr.*, 2008, **88**, 855S–858S.
5 M. Manto, Abnormal Copper Homeostasis: Mechanisms and Roles in Neurodegeneration, *Toxics*, 2014, **2**, 327–345.
6 H. Kozlowski, M. Luczkowski, M. Remelli and D. Valensin, Copper, zinc and iron in neurodegenerative diseases (Alzheimer's, Parkinson's and prion diseases), *Coord. Chem. Rev.*, 2012, **256**, 2129–2141.
7 D. L. Sparks, C. Ziolkowski, D. Connor, T. Beach, C. Adler and M. Sabbagh, Copper and cognition in Alzheimer's disease and Parkinson's disease, *Cell Biol. Toxicol.*, 2008, **24**, 426–430.
8 P. S. Donnelly, Z. G. Xiao and A. G. Wedd, Copper and Alzheimer's disease, *Curr. Opin. Chem. Biol.*, 2007, **11**, 128–133.
9 R. Hueting, Radiocopper for the imaging of copper metabolism, *J. Labelled Compd. Radiopharm.*, 2014, **57**, 231–238.
10 J. T. Jørgensen, M. Persson, J. Madsen and A. Kjær, High tumor uptake of Cu-64: implications for molecular imaging of tumor characteristics with copper-based PET tracers, *Nucl. Med. Biol.*, 2013, **40**, 345–350.
11 G. J. Brewer, S. H. Kanzer, E. A. Zimmerman, D. F. Celmins, S. M. Heckman and R. Dick, Copper and ceruloplasmin abnormalities in Alzheimer's disease, *Am. J. Alzheimer's Dis. Other Demen.*, 2010, **25**, 490–497.
12 G. J. Brewer, Alzheimer's disease causation by copper toxicity and treatment with zinc, *Front. Aging Neurosci.*, 2014, **9**, 1–5.
13 Y. H. Hung, A. I. Bush and R. A. Cherny, Copper in the brain and Alzheimer's disease, *J. Biol. Inorg. Chem.*, 2010, **15**, 61–76.
14 K. M. Davies, J. F. B. Mercer, N. Chen and K. L. Double, Copper dyshomoeostasis in Parkinson's disease: implications for pathogenesis and indications for novel therapeutics, *Clin. Sci.*, 2016, **130**, 565–574.
15 R. Bahde, S. Kapoor, K. K. Bhargava, M. L. Schilsky, C. J. Palestro and S. Gupta, PET with ^{64}Cu–histidine for noninvasive diagnosis of biliary copper excretion in Long–Evans Cinnamon rat model of Wilson disease, *J. Nucl. Med.*, 2012, **53**, 961–968.

16 F. Peng, S. Lutsenko, X. K. Sun and O. Muzic, Positron emission tomography of copper metabolism in the ATP7b$^{-/-}$ knock-out mouse model of Wilson's disease, *Mol. Imaging Biol.*, 2012, **14**, 70–78.

17 F. Peng, Positron emission tomography for measurement of copper fluxes in live organisms, *Ann. N. Y. Acad. Sci.*, 2014, **1314**, 24–31.

18 F. Peng, X. Lu, J. Janisse, O. Muzik and A. F. Shields, Positron emission tomography of human prostate cancer xenografts in mice with increased uptake of copper(II)-64 chlorides, *J. Nucl. Med.*, 2006, **47**, 1649–1652.

19 H. Zhang, H. Cai, X. Lu, O. Muzik and F. Peng, Positron emission tomography of human hepatocellular carcinoma xenografts in mice using copper(II)-64 chloride as a tracer, *Acad. Radiol.*, 2011, **18**, 1561–1568.

20 H. H. W. Chen and M. T. Kuo, Overcoming platinum drug resistance with copper-lowering agents, *Anticancer Res.*, 2013, **33**, 4157–4161.

21 L.-M. Wang, J. S. Becker, Q. Wu, M. F. Oliveira, F. A. Bozza, A. L. Schwager, J. M. Hoffman and K. A. Morton, Bioimaging of copper alterations in the aging mouse brain by autoradiography, laser ablation inductively coupled plasma mass spectrometry and immunohistochemistry, *Metallomics*, 2010, **2**, 348–353.

22 M. T. Fodero-Tavoletti, V. L. Villemagne, B. M. Paterson, A. R. White, Q.-X. Li, J. Camakaris, G. J. O'Keefe, R. Cappai, K. J. Barnham and P. S. Donnelly, Bis(thiosemicarbazonato) Cu-64 Complexes for Positron Emission Tomography Imaging of Alzheimer's Disease, *J. Alzheimer's Dis.*, 2010, **20**, 49–55.

23 J. B. Torres, E. M. Andreozzi, J. T. Dunn, M. Siddique, I. Szanda, D. R. Howlett, K. Sunassee and P. J. Blower, PET Imaging of Copper Trafficking in a Mouse Model of Alzheimer's Disease, *J. Nucl. Med.*, 2016, **57**, 109–114.

24 J. L. J. Dearling, J. S. Lewis, D. W. McCarthy, M. J. Welch and P. J. Blower, Redox-active metal complexes for imaging hypoxic tissues: structure-activity relationships in copper(II) bis(thiosemicarbazone) complexes, *Chem. Commun.*, 1998, 2531–2532.

25 J. L. J. Dearling, J. S. Lewis, G. E. D. Muller, M. J. Welch and P. J. Blower, Copper bis(thiosemicarbazone) complexes as hypoxia imaging agents: structure-activity relationships, *J. Biol. Inorg. Chem.*, 2002, **7**, 249–259.

26 M. S. Cooper, M. T. Ma, K. Sunassee, K. P. Shaw, J. D. Williams, R. L. Paul, P. S. Donnelly and P. J. Blower, Comparison of ^{6}4Cu-complexing bifunctional chelators for radioimmunoconjugation: labeling efficiency, specific activity, and *in vitro*/*in vivo* stability, *Bioconjugate Chem.*, 2012, **23**, 1029–1039.

27 S. Walker-Samuel, R. Ramasawmy, F. Torrealdea, M. Rega, V. Rajkumar, S. P. Johnson, S. Richardson, M. Gonçalves, H. G. Parkes, E. Årstad, D. L. Thomas, R. B. Pedley, M. F. Lythgoe and X. Golay, *In vivo* imaging of glucose uptake and metabolism in tumors, *Nat. Med.*, 2013, **19**, 1067–1072.

28 C. J. Mathias, M. J. Welch, M. A. Green, H. Diril, C. F. Meares, R. J. Gropler and S. R. Bergmann, *In vivo* comparison of copper blood-pool agents: potential radiopharmaceuticals for use with copper-62, *J. Nucl. Med.*, 1991, **32**, 475–480.

29 R. Hueting, V. Kersemans, B. Cornelissen, M. Tredwell, K. Hussien, M. Christlieb, A. D. Gee, J. Passchier, S. C. Smart, J. R. Dilworth, V. Gouverneur and R. J. Muschel, A comparison of the behavior of ^{64}Cu-acetate and ^{64}Cu-ATSM *in vitro* and *in vivo*, *J. Nucl. Med.*, 2014, **55**, 128–134.

30 F. Peng, J. Liu, J.-S. Wu, X. Lu and O. Muzik, Mouse extrahepatic hepatoma detected on microPET using copper(II)-64 chloride uptake mediated by endogenous mouse copper transporter 1, *Mol. Imaging Biol.*, 2005, **7**, 325–329.

31 A. R. Jalilian, S. Shanesazzadeh, P. Rowshanfarzad, F. Bolourinovin and A. Majdabad, Biodistribution study of [Cu-61]pyruvaldehyde-bis(*N*-4-methylthiosemicarbazone) in normal rats as a PET tracer, *Nucl. Sci. Tech.*, 2008, **19**, 159–164.

32 T. C. Castle, R. I. Maurer, F. E. Sowrey, M. J. Went, C. A. Reynolds, E. J. L. McInnes and P. J. Blower, Hypoxia-targeting copper bis(selenosemicarbazone) complexes: comparison with their sulfur analogues, *J. Am. Chem. Soc.*, 2003, **125**, 10040–10049.

33 C. A. Owen Jr., *Biochemical aspects of copper: copper proteins, ceruloplasmin, and copper protein binding*, Noyes Publications, Park Ridge, New Jersey, 1982, pp. 177–181.

34 J. L. J. Dearling and A. B. Packard, On the destiny of copper species, *J. Nucl. Med.*, 2014, **55**, 7–8.

35 M. C. Linder, L. Wooten, P. Cerveza, S. Cotton, R. Shulze and N. Lomeli, Copper transport, *Am. J. Clin. Nutr.*, 1998, 965S–971S.

36 B.-S. Choi and W. Zheng, Copper transport to the brain by the blood-brain barrier and blood-CSF barrier, *Brain Res.*, 2009, 14–21.

37 J. B. Torres, PhD thesis, King's College London, 2017.

38 Y. Pushkar, G. Robison, B. Sullivan, S. X. Fu, M. Kohne, W. Jiang, S. Rohr, B. Lai, M. A. Marcus, T. Zakharova and W. Zheng, Aging results in copper accumulations in glial fibrillary acidic protein-positive cells in the subventricular zone, *Aging Cell*, 2013, **12**, 823–832.

39 D. Hare, J. K. Lee, A. D. Beavis, A. van Gramberg, J. George, P. A. Adlard, D. I. Finkelstein and P. A. Doble, Three-dimensional atlas of iron, copper, and zinc in the mouse cerebrum and brainstem, *Anal. Chem.*, 2012, **84**, 3990–3997.

40 N. Nishimura, H. Nishimura, A. Ghaffar and C. Tohyama, Localization of Metallothionein in the Brain of Rat and Mouse, *J. Histochem. Cytochem.*, 1992, **40**, 309–315.

41 N. A. Platonova, S. V. Barabanova, R. G. Povalikhin, N. V. Tsymbalenko, M. A. Danilovskii, O. V. Voronina, I. I. Dorokhova and L. V. Puchkova, *In vivo* expression of copper-transporting proteins in rat brain regions, *Biol. Bull.*, 2005, **32**, 108–120.

42 C. J. Mathias, M. J. Welch, M. E. Raichle, M. A. Mintun, L. L. Lich, A. H. McGuire, K. R. Zinn, E. K. John and M. A. Green, Evaluation of a potential generator-produced PET tracer for cerebral perfusion imaging – single-pass

cerebral extraction measurements and imaging with radiolabeled Cu-PTSM, *J. Nucl. Med.*, 1990, **31**, 351–359.

43 T. R. Wallhaus, J. Lacy, J. Whang, M. A. Green, R. J. Nickles and C. K. Stone, Human biodistribution and dosimetry of the PET perfusion agent copper-62-PTSM, *J. Nucl. Med.*, 1998, **39**, 1958–1964.

44 D. P. Holschneider, J. Yang, T. R. Sadler, N. B. Galifianakis, M. H. Bozorgzadeh, J. R. Bading, P. S. Conti and J. M. I. Maarek, Changes in regional brain perfusion during functional brain activation: comparison of [Cu-64]-PTSM with [C-14]-Iodoantipyrine, *Brain Res.*, 2008, **1234**, 32–43.